# Identification of network-level coding units for real-time representation of episodic experiences in the hippocampus

**Longnian Lin*†‡§, Remus Osan*‡§, Shy Shoham‡, Wenjun Jin*‡, Wenqi Zuo*‡, and Joe Z. Tsien*‡¶**

*Center for Systems Neurobiology, Departments of Pharmacology and Biomedical Engineering, Boston University, Boston, MA 02118; †Shanghai Institute of Brain Functional Genomics, East China Normal University, Shanghai 200062, China; and ‡Department of Molecular Biology, Princeton University, Princeton, NJ 08544-1014

Edited by Thomas C. Südhof, University of Texas Southwestern Medical Center, Dallas, TX, and approved March 1, 2005 (received for review November 4, 2004)

**To examine the network-level organizing principles by which the brain achieves its real-time encoding of episodic information, we have developed a 96-channel array to simultaneously record the activity patterns of as many as 260 individual neurons in the mouse hippocampus during various startling episodes. We find that the mnemonic startling episodes triggered firing changes in a set of CA1 neurons in both startle-type and environment-dependent manners. Pattern classification methods reveal that these firing changes form distinct ensemble representations in a low-dimensional encoding subspace. Application of a sliding window technique further enabled us to reliably capture not only the temporal dynamics of real-time network encoding but also postevent processing of newly formed ensemble traces. Our analyses revealed that the network-encoding power is derived from a set of functional coding units, termed neural cliques, in the CA1 network. The individual neurons within neural cliques exhibit ''collective cospiking'' dynamics that allow the neural clique to overcome the response variability of its members and to achieve real-time encoding robustness. Conversion of activation patterns of these coding unit assemblies into a set of real-time digital codes permits concise and universal representation and categorization of discrete behavioral episodes across different individual brains.**

episodic memory | neural clique | neural code | startle | cell assembly

Understanding the network-level organizing principles that allow the brain to form real-time neural representations of episodic experiences is a central issue in neuroscience. Anatomically, the hippocampus, and especially its CA1 subregion, is known to be a crucial site for the formation of episodic memories of events and places (1–6). In fact, individual hippocampal neurons have been shown to respond to many external inputs (7–13). Yet, the response variability at the level of individual neurons poses a theoretical obstacle to the understanding how the brain achieves its robust real-time neural coding of the stimulus representation (14–16). It has been long thought that mnemonic encoding of information may involve the coordinated activity of large numbers of individual neurons (17, 18). However, virtually little is known about the actual real-time network-level encoding patterns and their underlying organizing principles and mechanisms.

To study these issues, we have developed a high-density recording technique for mice in which sophisticated genetic analyses of cognitions are feasible (19, 20). In parallel, we have also designed a set of simple, and yet robust, behavioral paradigms by using startling episodes. We reasoned that such episodic events are likely to involve large numbers of neurons, thereby greatly increasing the chance of finding them simultaneously and, consequently, facilitating the analysis of network-level real-time encoding patterns in the brain. Here, we report on our experimental measurements and mathematical descriptions of CA1-encoding patterns associated with various mnemonic startling episodes, as well as on the identification of functional coding units, termed neural cliques, in the hippocampal network. Furthermore, we describe a way to convert the real-time activation patterns of neural clique assemblies to an invariant binary code for categorizing and representing episodic information across different individual brains.

## Materials and Methods

***In Vivo* Recording and Spike Sorting.** The 96-channel recording array (in stereotrode format) was constructed and implanted onto the head of B6BCA/J mice. The electrodes were advanced slowly until reaching the CA1. The spike activities in freely behaving mice in response to various startling episodes such as an air blow to the animal's back, free fall of the animal while inside a small elevator, or earthquake-like cage shake were recorded by Plexon Systems (Dallas) and then sorted by using the MCLUST3.0 and KLUSTAKWIK 1.5 programs (21). Only stable units (for at least 6 h) with clear boundaries and <0.5% of spike intervals within a 1-ms refractory period are included in the present analysis.

**Data Analysis.** The firing rates of each neuron during the 1 s that followed the startle stimuli were computed by using two 500-ms time bins ($f_{\text{poststartle, }n}$). The neural responses were obtained by using $R_n = (f_{\text{poststartle, }n} - f_{\text{pre}})/(f_o + f_{\text{pre}})$, where $f_{\text{pre}}$ is the prestimulus baseline firing rate and $f_o$ is the global mean response frequency of the recorded excitatory neuron (2–3 Hz). Multiple discriminant analysis (MDA) (22) was used to compute a highly informative low-dimensional subspace that allows discriminating among the different startling episodes. Projections of training data points in this subspace were fit with multivariate Gaussian distributions:

$$P(x) = \frac{1}{(2\pi)^{N/2}|\Sigma|^{1/2}} \exp(-(x-m)'\Sigma^{-1}(x-m)/2)$$

to compute prediction of class membership for test data points (leave-one-out method). Hierarchical clustering (22) was used to group neurons with similar response properties as a way of identifying encoding units in CA1. The MDA ensemble responses were then mapped into a startle-selective encoding coordinate system to obtain efficient and universal binary codes for categorizing startle episodes across different animals.

For a detailed description of construction of 96-channel ensemble recording array (Fig. 6, which is published as support-

This paper was submitted directly (Track II) to the PNAS office.

Abbreviation: MDA, multiple discriminant analysis.

§L.L. and R.O. contributed equally to this work.

¶To whom correspondence should be addressed. E-mail: jtsien@bu.edu.

ing information on the PNAS web site), *in vivo* recording and spike sorting (Figs. 7 and 8, which are published as supporting information on the PNAS web site), behavioral tests of startling memories, and data analysis, please see *Supporting Text*, which is published as supporting information on the PNAS web site.

## Results

**Ensemble Patterns of CA1 Single-Unit Activity Triggered by Startling Events.** Because the brain can produce robust episodic memories of startling events (e.g., devastating earthquakes, roller coaster rides, shark attack, etc.) even upon a single exposure (23–25), we have correspondingly designed a set of behavioral paradigms and used three different types of startling stimuli delivered to the mice as a way of creating discrete episodic startle memories: air blow, a sudden blow of air to the animal's back (mimicking an owl attack from sky); drop, a short vertical free fall inside a small elevator (recreating the mouse's experiences inside a cookie jar that falls from a kitchen shelf); and shake, an unexpected brief earthquake-like shaking of the mouse's cage. We used computer-controlled mechanical devices for controlling the precise timing and intensity of these startling stimuli. Such startling episodic events are capable of producing robust startle memories, as evident from our measurements of the 3-h retention of place conditioning memory (Fig. 9, which is published as supporting information on the PNAS web site).

We simultaneously recorded 260, 210, 148, and 138 individual CA1 units in mice A, B, C, and D, respectively, while subjecting them to seven repetitions of each of the above-mentioned startling stimuli. These stimuli produced collective changes in firing rates and activity patterns within a subset of the recorded neuronal populations. As an example, the spike rasters of 260 simultaneously recorded single units from mouse A show dynamical changes in the firing patterns of many CA1 neurons after the occurrence of single startling episodes of air blow, drop, and shake (Fig. 1).

**Diversity in CA1 Cell Response Selectivity to Startling Episodes.** To analyze the neural basis underlying the formation of episodic memory, we first examined the temporal dynamics of each individual CA1 cell in response to a variety of startling events. Although a significant proportion of the simultaneously recorded CA1 cells did not respond to any of the startle stimuli, the remainder exhibited significant changes in firing rates. In general, based on their temporal response duration, dynamical changes triggered by startling episodes can be generally divided into four major firing modes: transient increase, transient decrease, prolonged increase, and prolonged decrease (see Fig. 10, which is published as supporting information on the PNAS web site). The transient changes were as short as 250 ms or less, whereas the prolonged increases lasted up to 40 s in duration.

Of the total of 756 single units recorded (pooled from four animals), 13.5% exhibited transient increases, 31.7% showed prolonged increases, 1.9% had transient decreases, and 1.4% responded with a prolonged decrease in their firing frequency. Thus, the ratio of neurons showing increased vs. decreased firing is ≈14 to 1. We further note that although the spike discharge frequency and interspike-intervals of these individual neurons were quite variable across repetitions (for several examples, see peri-event spike rasters in Fig. 2; see also Fig. 10), response modes to the same type of startle were almost always consistent in terms of their temporal dynamics (i.e., transient vs. prolonged, increase vs. decrease).

We then analyzed the response-selectivity of these CA1 cells. Spike-raster plots and peri-event histograms reveal that some of these CA1 neurons responded to all three types of startling events (Fig. 2*A*, general startle cells), whereas other cells appeared to only respond to air blow, drop, or shake (Fig. 2 *B–D*). Importantly, we have also observed many CA1 cells that reacted to combinations of two different types of startles, responding to both startles either equally or differentially (Fig. 2 *E* and *F*), thereby reflecting the hippocampal binding function of cortical inputs. This diversity of response-specificity suggests that the startling events are likely to be represented in CA1 by activity patterns of unique ensembles of neurons.

**Effects of Environmental Contexts on Startle-Induced Individual Neuronal Responses.** Because the hippocampus is involved in the formation of episodic memory that contains not only "what" information but also "where" information (1–5, 8), we next asked to what extent the firing patterns of CA1 cells triggered by startling events are influenced by the environmental contexts in which the startles occur. To address this question, we repeated the sudden air blow stimuli in two distinct cages and the drop stimuli in two different elevators. Although a given type of startling stimuli triggered similar responses in many of the responsive CA1 units regardless of the environmental context (Fig. 2 *G* and *H*), some CA1 cells exhibited context-specific firing changes (Fig. 2 *I* and *J*). Thus, these contextual experiments demonstrate that the startle-triggered firing changes in some CA1 neurons are not only stimulus-dependent, but also depend on the context in which the event occurs, thereby reflecting a clear neural integration of both what and where information in

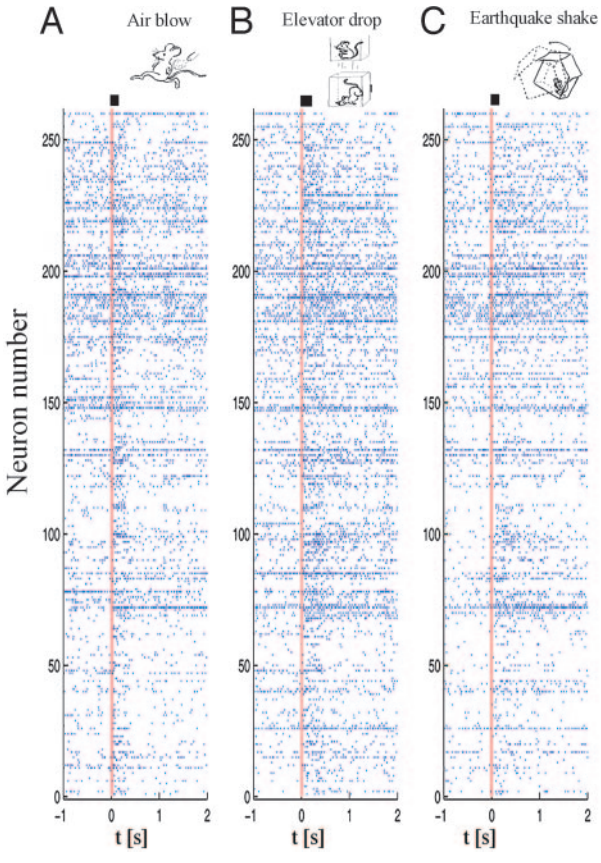


**Fig. 1.** Startle-induced ensemble of single-unit firing patterns in CA1. Spike rasters of 260 simultaneously recorded single units from mouse A during a period of 1 s before and 2 s after the occurrence of single startling episodes of air blow (*A*), drop (*B*), and shake (*C*) ($t = 0$ marked with vertical red line). *x* axis, time scale (seconds); *y* axis, the numbers of simultaneously recorded single units ($n = 260$). The startle stimulus durations are indicated as a bar next to the vertical red line above the spike raster. Although many neurons did not respond to startling stimuli, a significant portion of recorded units exhibited dynamical changes in their firing rates.

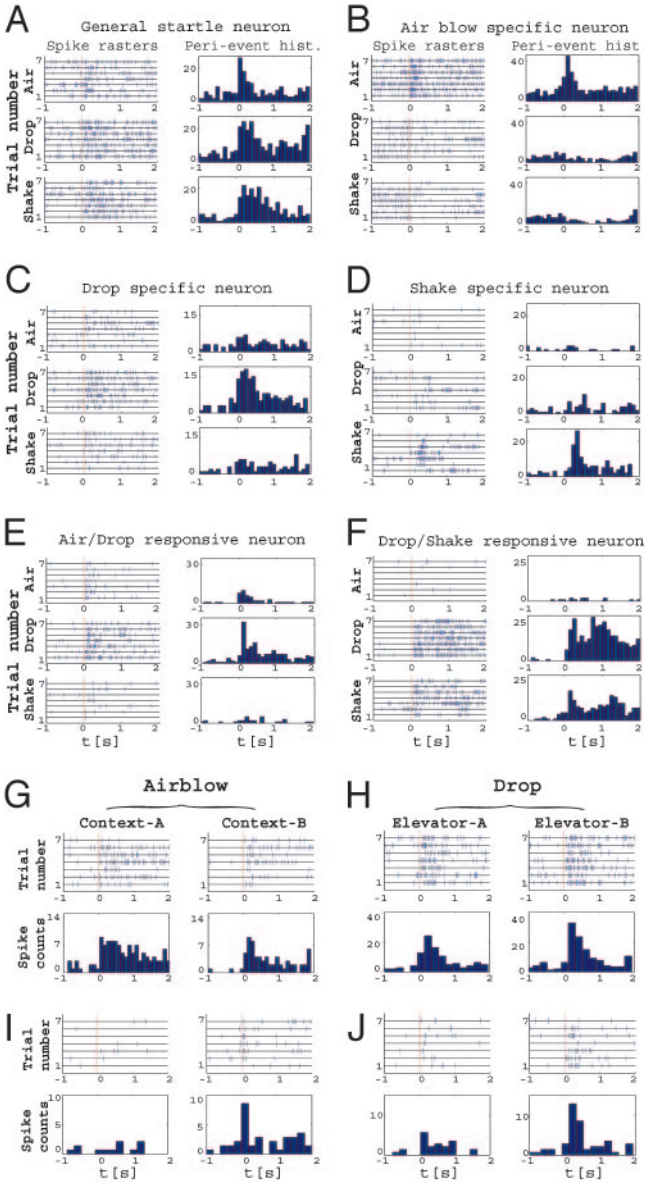


**Fig. 2.** Diversity and selectivity of CA1 neuronal responses to different startle stimuli. Spike raster plots and peri-event histograms (time bin, 100 ms) for representative units are shown. In *A–F*, *Top*, *Middle*, and *Bottom* correspond to air, drop and shake events, respectively. (*A*) A unit responsive to all three types of startles (general-startle unit). (*B*) A unit that increased its firing selectively to air blow (air-blow unit). (*C*) Drop-selective unit. (*D*) Shake-selective unit. (*E*) Air- and drop-responsive unit. (*F*) Drop- and shake-responsive unit. (*G*) A unit that responded to air blows in both contexts. (*H*) A unit that responded only in context B. (*I*) A unit that responded to drop similarly in elevator A and in elevator B. (*J*) A unit that exhibited a strong drop response only in Elevator B. All histograms use a time bin of 200 ms. Please note the response variability of each individual neuron across the repeating seven trials (*y* axis). *x* axis indicates the time scale (seconds). The vertical red lines in spike rasters indicate the time marker for the occurrence of startling events.

the hippocampal region, a hallmark mnemonic function of the hippocampus (1, 2).

**Ensemble Pattern Classification and Visualization of CA1 Network Encoding.** The existence of a variety of responsive individual neurons suggests that startling events may be represented through distinct activity patterns at the network level by an ensemble of individual neurons. What are those ensemble encoding patterns? How can these encoding patterns be mathematically described and even visualized? To provide an intuitive solution that would facilitate a search for the relevant network-encoding patterns that might be hidden among the activity of the hundreds of simultaneous recorded neurons we used MDA (22) to compute a highly informative low-dimensional subspace among the firing patterns of responsive neurons. MDA is a supervised dimensionality-reduction method that is well suited for identifying and integrating the classification-significant statistical features of neural population responses to distinct types of known stimuli.

In our implementation of MDA, a startle trial was represented as a high-dimensional feature vector of normalized neural responses $R_n = (f_{\text{poststartle},\,n} - f_{\text{pre}})/(f_o + f_{\text{pre}})$. Each vector has $k = n \times m$ dimensions, where $n$ is the number of CA1 neurons (e.g., in Mouse A, $n = 260$), and $m$ is the number of time bins (e.g., $m = 2$ for 500 ms over a 1-s response period). Responses that fell below a threshold criterion were eliminated, leading to a sparse set of neural features included in the analysis (for example, in mouse A of the $260 \times 2$ features, 185 features with $R > 0.5$ were used, with 160 features selected from the first 500-ms poststimulus bins and 25 feature vectors from the second 500-ms bins). In other words, the nonresponsive neurons are excluded because they are unlikely to carry neural information; as a result only the responsive neurons are used for MDA analysis.

Next, we calculated the low-dimensional MDA subspace that is maximally discriminating for the response matrix (see *Supporting Text*). Projecting the neural population responses to given startle events onto single points in this subspace shows that repeated startle responses form clearly well separated clusters (Fig. 3*A*), which are distinct from the cluster formed by the rest projections. In other words, CA1 ensemble activity patterns elicited by various startling stimuli can be mathematically described and conveniently visualized as specific startle clusters in a low-dimensional encoding subspace (here in three dimensions), achieving levels of startle discrimination not seen in individual CA1 neuron responses. In addition, air blow and drop environmental context representations can be further separated by using two additional classification steps (Fig. 3 *B* and *C*, respectively). We also confirmed that nonresponsive cells indeed did not contribute to these classifications as adding them to MDA analysis did not significantly change the MDA patterns (data not shown).

How well can the population encoding patterns predict behavioral startle identity? To address this question, we fit the clusters formed by training data with Gaussian ellipsoids (two standard-deviation boundaries are indicated in Fig. 3*A*) and calculated the probabilities that the test points belong to the correct class by employing a cross-validation method (no test data were used in the training). The classification results (Table 1, based on a variation of the leave-one-out cross-validation method) indicate that the prediction accuracy is typically >90% and in nearly all of our recordings is >80% (overall mean 92%).

To further confirm our finding that various startle-triggered ensemble responses of individual CA1 neurons form distinct encoding patterns in low-dimensional subspaces, we used an independent classification method, known as principal component analysis (PCA) to analyze the data sets. PCA is an unsupervised, linear dimensionality reduction tool that is often used for identifying the structure that best represents the data in a least-square sense (22). Similar to our observations from MDA analysis, the distinct encoding structure of the CA1 population patterns is revealed again by using this independent dimensionality-reduction method (see Fig. 11 and Table 2, which are published as supporting information on the PNAS web site).

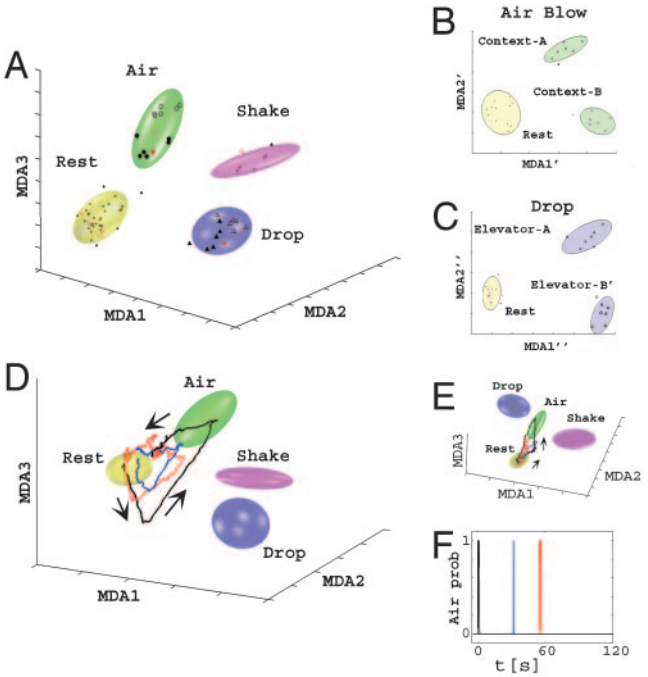


**Fig. 3.** Classification, visualization, and dynamical decoding of CA1 ensemble representations of startle episodes by MDA methods. (*A*) Firing patterns during rest (dots, yellow ellipsoid), air blow (circles, green ellipsoid), drop (triangles, blue ellipsoid), and shake (stars, magenta ellipsoid) epochs are shown after being projected to a three-dimensional space obtained by using MDA for mouse A; MDA1–3 denote the discriminant axes. Both training (dark symbols) and test (red symbols) data are shown. After the identification of startle types, a subsequent MDA is further used to resolve contexts (full vs. empty symbols) in which the startle occurred for air-blow context (*B*) and for elevator drop (*C*). (*D*) Dynamical monitoring of ensemble activity and the spontaneous reactivation of startle representations. Three-dimensional subspace trajectories of the population activity in the two minutes after an air-blow startle in mouse A are shown. The initial response to an air blow (black line) is followed by two large spontaneous excursions (blue and red lines), characterized by coplanar, geometrically similar lower amplitude trajectories (directionality indicated by arrows). (*E*) The same trajectories of *A* from a different 3D angle. (*F*) The timing ($t_1 = 31.6$ s and $t_2 = 54.8$ s) of the two reactivations (marked in blue and red, respectively) after the actual startle (in black) ($t = 0$ s). The vertical axis indicates the air-blow classification probability.

**Monitoring of Real-Time Encoding and Dynamical Postevent Processing of CA1 Network Traces.** MDA provides a sensitive and mathematical means of measuring and visualizing the ensemble neural activity patterns in a highly informative encoding subspace. This dimensionality-reduction method can further be used to dynamically monitor the population firing patterns by using a sliding-window technique (1-s width; see *Supporting Text*). Using the fixed matrix coefficients produced by the MDA method, we can compute the instantaneous projection of neural responses during the entire experiment. As such, the temporal evolution of the ensemble activity patterns can be directly visualized as dynamical trajectories in the encoding subspace. For example, during the baseline state before startles, the instantaneous projection was confined to the rest ellipsoid; however, upon the actual startling stimulus, we observe a planar trajectory that begins in the rest cluster, quickly visits the corresponding startle cluster, and then returns to rest (an example for air blow is shown in Fig. 3 *D–F*, and for drop, black trajectories, see Fig. 12, which is published as supporting information on the PNAS web site).

Intriguingly, using this approach, we further observed spontaneous excursions from the rest ellipsoid during the poststartling event period (Fig. 3*D*). These intrinsic excursions occurred in all four animals and had the directional specificity as well as the characteristic geometric shape of the original startle trajectories. Moreover, their spontaneous trajectories took place on the similar time scale and were also confined in the same plane but typically with a smaller magnitude than the startle-evoked trajectories (Fig. 3 *D* and *E*, red and blue trajectories for reactivations after an air-blow episode). We also measured the time of these spontaneous excursions, which were observed to occur causally at several seconds to minutes, with apparently random intervals, after the actual startles (Fig. 3*F*). For example, the timing of the two reactivations after the actual air-blow startle shown in Fig. 3*D* is $t_1 = 31.6$ s (red trajectories) and $t_2 = 54.8$ s (blue trajectories) (Fig. 3*F*), whereas the timing of a reactivation in another case (drop) is at 107.9 seconds (Fig. 12). The number of reactivations that followed the original startles ranged between zero and five in our experiments. Therefore, our analyses have allowed us to monitor the dynamics of postevent spontaneous reactivations and processing of CA1 ensemble patterns.

**Identification of Functional Coding Units, Neural Cliques, in the CA1 Network.** Our finding that the representations of startle events form tight, well separated clusters in a low-dimensional encoding subspace prompted us to examine in detail which neurons in the CA1 population are responsible for encoding the different events and what essential features of the neural signals are used to accomplish that. Thus, we used agglomerative hierarchical clustering (22), a pattern classification method that can aggregate units by iteratively grouping together neurons with minimally distant responses. The clustering results reveal the existence of various neural groups, or neural cliques, with similar response properties (Fig. 4*A*). These neural cliques exhibited an increase in firing rate to all three types of startles (i.e., a "general startle clique"), to one type of startle (i.e., "air-blow clique," "drop clique," and "shake clique"), and to a subset of mixed startles (i.e., drop/shake clique, drop/air-blow clique, and air-blow/shake clique), respectively.

How significant a role do these neural cliques play in CA1 encoding classification? We evaluated the contribution of these

**Table 1. Prediction power in the MDA-computed encoding subspace for startle type and context**

| Mouse | Rest | Air blow | Air blow in context A | Air blow in context B | Drop | Drop in elevator A | Drop in elevator B | Shake |
|---|---|---|---|---|---|---|---|---|
| A | 99 | 99 | 99 | 94 | 99 | 91 | 98 | 98 |
| B | 99 | 99 | 94 | 95 | 97 | 92 | 93 | 93 |
| C | 99 | 99 | 91 | 92 | 99 | 80 | 87 | 90 |
| D | 99 | 90 | 91 | 75 | 96 | 66 | 75 | 83 |

Percent correct predictions were evaluated by using 1,000 random combinations of training/test data for each mouse. Test data was excluded from the training set. The startle type was first determined (columns: rest, air blow, drop, and shake), followed by context classification for air blow (context A or B) and drop (elevator A or B). Data sets contained 260, 210, 148, and 138 simultaneously recorded CA1 units in mice A, B, C, and D, respectively.

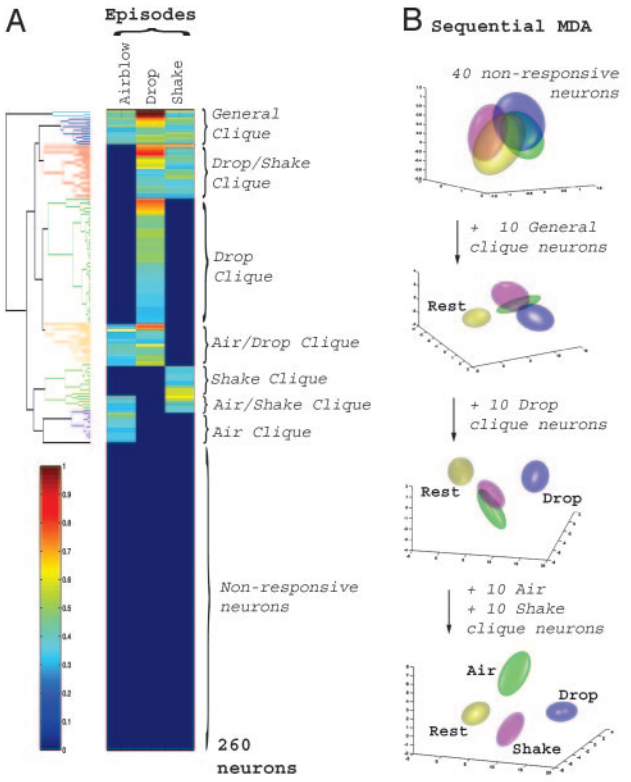


**Fig. 4.** Identification of functional encoding units in the CA1 cell assembly. (*A*) Hierarchical clustering of the responses of 260 simultaneously recorded neurons to the three different types of startles in mouse A reveals the existence of seven major neural cliques: general startle, drop–shake, drop, shake, shake–air blow, air blow, and air blow–drop (indicated by different colors on the dendrogram tree structure in *Left*). Nonresponsive units are grouped in the lower half. The color scale bar (*Left*) indicates the normalized response magnitude. (*B*) Discriminating power is derived from specific neural cliques. An initial group of 40 nonresponsive neurons is ineffective in producing discrimination (*Top*), whereas addition of the top 10 general startle clique neurons separates the rest cluster (yellow) from the startle clusters. Further inclusion of the top 10 drop clique neurons results in separation of the drop cluster (blue) from the still overlapping air-blow (green) and shake (magenta) clusters. The addition of the top 10 air-blow clique neurons and 10 shake clique neurons achieves full separation (*Bottom*) (see also Table 3). This application of MDA illustrates that these cliques play an important role in achieving discrimination for each category.

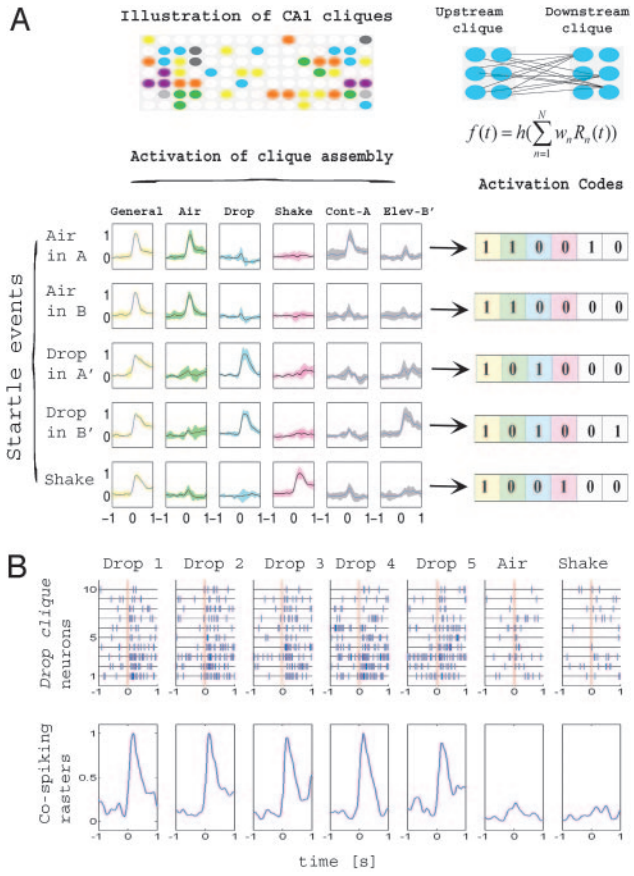


**Fig. 5.** Binary activation codes and real-time encoding robustness of neural cliques. (*A*) Conversion of activation patterns of neural clique assembly into real-time binary codes. Individual member neurons comprising neural cliques are illustrated by different colored circles. The activation function of a given clique at each network level can be mathematically described (equation in *Right*; also see Fig. 14, which is published as supporting information on the PNAS web site). Neural responses were weighted by using a remapping procedure and smoothed with a Gaussian filter ($\sigma = 100$ ms) as shown in *Left* ($\pm 1$ standard deviation confidence intervals are shown in corresponding colors). Rows correspond to the different startling episodes, whereas columns indicate the different neural cliques (general startle, air blow, drop, shake, air blow context A, and drop context B). The binary activation patterns corresponding to each event can be mathematically converted to a set of binary codes (*Bottom Right*, after the defined sequence of the cliques). As such, the clique activation codes are as follows: 110010 for air blow in context A, 110000 for air blow in context B, 101000 for drop in elevator A, 101001 for drop in elevator B, and 100100 for shake. Sparse membership distributions of CA1 neural cliques are illustrated (*Top Left*). (*B*) Real-time encoding robustness of neural cliques is derived from collective cospiking of its individual members. Spike rasters and weighted responses of the top 10 drop clique neurons (listed in *y* axis) during a drop event (1 s before and after the startle, *x* axis) are shown as an example. Although responses of the individual member (neuron) are quite variable from trial to trial, the consistency and specificity of the cospiking clique responses is evident from each drop episode (first five episodes are listed). The drop clique exhibited no significant responses to air-blow or shake episodes (*Bottom*, last two graphs on right). Robust cospiking of membership neurons in the cliques is also preserved at the finer time scale (20–30 ms) (see Fig. 13).

neural cliques to the startle representations by repeating the MDA analysis while sequentially adding clique members to an initial set of nonresponsive neurons. We find that a random selection of 40 nonresponsive cells as an initial set provides no discriminating power, yielding only overlapping representations (Fig. 4*B*). In contrast, inclusion of the 10 most responsive cells from the general startle clique leads to good separation between the rest cluster and the startle clusters but not among startle clusters. The selective discrimination of drop startles is obtained by the addition of as few as 10 top neurons from the drop clique. Similarly, the inclusion of 10 air-blow clique and 10 shake clique top neurons subsequently leads to full discrimination between all of the startle types. The increase in prediction power by the sequential addition of neural cliques is showed in Table 3, which is published as supporting information on the PNAS web site. In addition, we show that these 40 responsive neurons alone can achieve reliable classification of startle events (Table 3, last row). Thus, these 40 most responsive clique neurons are clearly capable of achieving accurate pattern classifications, whereas 40 unresponsive neurons provide essentially no discriminating power at the chance level. These findings suggest that these neural cliques constitute the basic functional coding units for encoding the identity of different startling episodes.

**Converting the Activation Pattern of Neural Cliques into a Real-Time Binary Code.** The MDA encoding subspace we have examined so far provides an efficient separation of the startle episodes based on the recorded ensemble activity patterns. However, in contrast

to the specificity exhibited by neural cliques, this MDA subspace does not show startle-type selectivity along any of its discriminant axes. To translate the ensemble responses into a startle-selective encoding coordinate system, we assigned new positions for the cluster centers so that they are linearly mapped into a clique-space, where each axis directly corresponds to a particular clique, thus projecting specific activation patterns to 1 and the absence of activation to 0. This mathematical operation achieves the reorientation of the main axes of the low-dimensional encoding subspace by inverting the matrix containing the centers of startle representations in that space (see *Supporting Text* for the matrix inversion step).

By projecting the ensemble patterns directly into this clique space, the recorded neural activities are now mapped onto a set of highly reproducible and selective responses. Each clique-space projection vector (columns in Fig. 5*A*) is clearly selective to a specific combination of startles (i.e., general-startle, air blow, drop, etc.), and does not respond to additional features. In addition, this selectivity also extends to the representation of contexts. Furthermore, the weights in the projection vectors strongly correlate with the responsiveness of neurons in the corresponding clique (data not shown). As a result, the activated cliques can be directly detected by using simple threshold crossing and, consequently, their collective identity uniquely codes for any given startle. For example, based on a predefined sequence of clique assembly (general-startle/air blow/drop/shake/air subcontext/drop subcontext), the activation code 110010 corresponds to the internal representation of the air blow in context A, 110000 to air blow in context B, 101000 to drop elevator A, 101001 to drop elevator B, and 100100 to shake.

Importantly, these binary codes can be dynamically implemented to detect the occurrence of the internal representations of startling episodes. For example, using the thresholded responses of these cliques, we can compute the "hit ratio" for correctly matching activation patterns with the binary codes. The prediction performance obtained by using these codes are the same to the ones listed in Table 1 (see also Table 4, which is published as supporting information on the PNAS web site).

Identification of neural cliques as the functional coding units for internal representation has prompted us to further look into the robustness of real-time encoding by neural cliques. This finding is a particularly important issue, as it is well known that a single neuron often shows large variations in both spike discharge and interspike intervals in response to repetition of identical stimuli (14–16). We found that these individual members within each clique fired tightly together in close temporal proximity during startle episodes. This collective cospiking feature allowed the neural cliques to overcome the response variability of their individual members and, thus, to achieve real-time encoding robustness. For example, the neural clique formed by the 10-drop neurons used in Fig. 4 consistently produced robust response to drops, but not to air blow or shake events (Fig. 5*B*). Further examination of their temporal dynamics at finer time scale (20–30 ms) again confirmed that the collective cospiking of these individual neurons has greatly enhanced real-time signal-to-noise robustness (Fig. 13, which is published as supporting information on the PNAS web site). Therefore, the cospiking of clique neurons is capable of providing a network-level mechanism for real-time encoding robustness and can act as a robust internal timer to reliably signal the occurrence of external events.

## Discussion

A central issue in the study of neural coding in the brain is the response variability of individual neurons (14–16). This variability at the level of individual neurons has posed a theoretical challenge for understanding how the brain achieves its real-time encoding and decoding of behavioral experiences. A traditional way to deal with this issue is to average the response of an individual neuron over many repetitions and trials. Although it allows the identification of event-related neural response, this practice of data averaging unfortunately loses crucial information regarding real-time neural coding functions. Here, we have described and visualized the network-level encoding patterns and postevent immediate processing of startling episodic experience in the CA1 region of the hippocampus. We have further identified network-level functional coding units capable of overcoming the response variability of individual neurons and achieving real-time network representation of startling episodic experiences. It would be of interest to investigate how the individual neurons that comprise a functional coding clique are anatomically connected and how they are modulated by synaptic plasticity (26–28), and to further dissect to what extent they reflect the sensory, emotional, mnemonic, or even conceptual aspects of the events (7, 23). Nonetheless, when the activation patterns of these coding units are converted (29) into a set of concise digital codes, they seem to permit universal representation and categorization of discrete behavioral episodes across different animals. Therefore, the "neural clique cospiking" principle provides a plausible network-level basis by which the nervous systems can achieve real-time neural coding and processing of behavioral information. For more discussion on our findings, see *Extended Discussion* in *Supporting Text*.

We thank Yuan Liu and Kim Zaia for assistance and Dr. Gyorgy Buszaki and his staff for providing advice on the ensemble recordings. This research was supported by funds from National Institutes of Health Grants MH60236, MH61925, MH62632, and AG02022, the Burroughs Wellcome Fund, ECNU Award TY04610, Ministry of Science and Technology of China Program Project 973, and the W. M. Keck Foundation (all to J.Z.T.).

1. Squire, L. R. (1987) *Memory and Brain* (Oxford Univ. Press, Oxford).
2. Cohen, N. J. & Eichenbaum, H. (1993) *Memory, Amnesia, and the Hippocampal System* (MIT Press, Cambridge, MA).
3. Rudy, J. W., Barrientos, R. M. & O'Reilly, R. C. (2002) *Behav. Neurosci.* **116,** 530–538.
4. Rampon, C., Tang, Y. P., Goodhouse, J., Shimizu, E., Kyin, M. & Tsien, J. Z. (2000) *Nat. Neurosci.* **3,** 238–244.
5. Sara, S. J. (2000) *Learn. Mem.* **7,** 73–84.
6. Wittenberg, G. M. & Tsien, J. Z. (2002) *Trends Neurosci.* **25,** 501–505.
7. Berger, T. W., Alger, B. & Thompson, R. F. (1976) *Science* **192,** 483–485.
8. O'Keefe, J. & Nadal, L. (1978) *The Hippocampus as a Cognitive Map* (Oxford Univ. Press, Oxford).
9. Weiss, C., Kronforst-Collins, M. A. & Disterhoft, J. F. (1996) *Hippocampus* **6,** 192–209.
10. Deadwyler, S. A., Bunn, T. & Hampson, R. E. (1996) *J. Neurosci.* **16,** 354–372.
11. Wilson, M. A. & McNaughton, B. L. (1994) *Science* **265,** 676–679.
12. Wirth, S., Yanike, M., Frank, L. M., Smith, A. C., Brown, E. N. & Suzuki, W. A. (2003) *Science* **300,** 1578–1581.
13. Dragoi, G., Harris, K. D. & Buzsaki, G. (2003) *Neuron* **39,** 843–853.
14. Lestienne, R. (2001) *Prog. Neurobiol.* **65,** 545–591.
15. Abbott, L. F. & Dayan, P. (1999) *Neural Comput.* **11,** 91–101.
16. Fenton, A. A. & Muller, R. U. (1998) *Proc. Natl. Acad. Sci. USA* **95,** 3182–3187.
17. Hebb, D. O. (1949) *The Organization of Behavior* (Wiley, New York).
18. Abbott, L. E. & Sejnowski, T. J. (1999). *Neural Codes and Distributed Representations* (MIT Press, Cambridge, MA).
19. Shimizu, E., Tang, Y. P., Rampon, C. & Tsien, J. Z. (2000) *Science* **290,** 1170–1174.
20. Wang, H., Shimizu, E., Tang, Y.-P., Cho, M., Kyin, M., Zuo, W., Robinson, D. A., Alaimo, P. J., Zhang, C., Morimoto, H., *et al.* (2003) *Proc. Natl. Acad. Sci. USA* **100,** 4287–4292.
21. Csicsvari, J., Hirase, H., Czurko, A. & Buzsaki, G. (1998) *Neuron* **21,** 179–189.
22. Duda, R. O., Hart, E. P. & Stork, D. G. (2001) *Pattern Classification* (Wiley, New York)
23. Koch, M. (1999) *Prog. Neurobiol.* **59,** 107–128.
24. Davis, M., Hitchcock, J. & Rosen, J. B. (1987) *The Psychology of Learning and Memory*, ed. Bower, G. H. (Academic, New York).
25. LeDoux, J. E. (1994) *Sci. Am.* **270,** 50–57.
26. Wigstrom, H. & Gustafsson, B. (1985) *Acta Physiol. Scand.* **123,** 519–522.
27. Malenka, R. C. & Nicoll, R. A. (1999) *Science* **285,** 1870–1874.
28. Tsien, J. Z. (2000) *Sci. Am.* **282,** 62–68.
29. McCulloch, W. S. & Pitts, W. (1943) *Bull. Math. Biol.* **52,** 99–115.

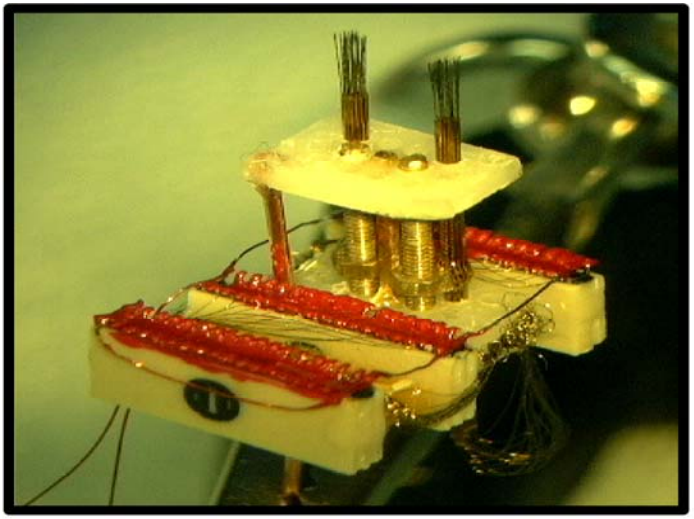

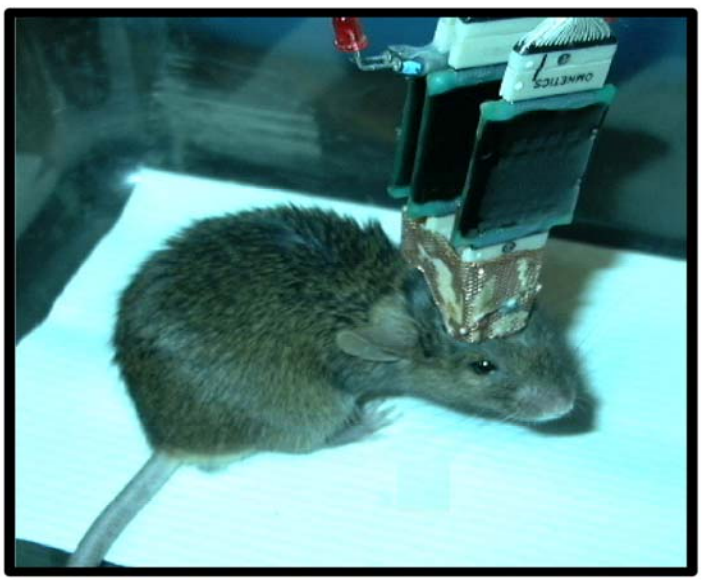

Supporting Figure 6

**Fig. 6.** A 96-channel headstage for *in vivo* recording in freely behaving mice. Construction of a 96-channel headstage for an extracellular *in vivo* recording headstage in progress (*Left*). Two 48-bundles of polyimide tubing have been glued to independently moveable screws. The distance between two bundles were precalculated to allow bilateral recording in the both the right and left side of the dorsal hippocampus. Within the bundle, each stereotrode has been threaded through a piece of the polyiimide tubing. *Upper Right* shows a completed 96-channel headstage; *Bottom Right* shows that a mouse implanted with our lightweight headstage can perform various behavioral tasks.

A

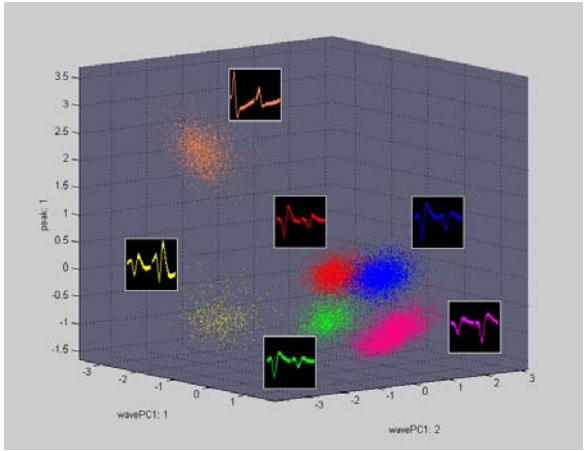


B

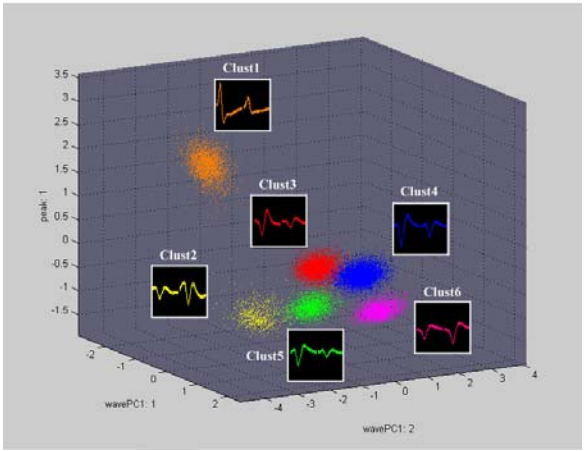


C

| | L-Ratio | Isolation Distance (ID) |
|---|---|---|
| Clust 1 | 0.0045 | 184.4 |
| Clust 2 | 0.0005 | 118.7 |
| Clust 3 | 0.0036 | 85.3 |
| Clust 4 | 0.0062 | 79.5 |
| Clust 5 | 0.0049 | 54.6 |
| Clust 6 | 0.0155 | 218.4 |
| Average | 0.0058 | 123.4833 |

Supporting Figure 7

**Fig. 7.** Stability of recorded units. (*A*) Automatic spike sorting was performed by using the KLUSTAKWIK method and was followed by the MCLUST method for manual cluster cutting and merging. Six sorted units detected by a stereotrode are presented here in different colors. The stereotrode waveforms (the waveforms of each unit detected by each tip of the stereode, shown side-by-side) of the individual units are shown along the corresponding clusters. (*B*) The same six stable units at the completion of 6 h recording. (*C*) Quantitative measures of the quality of these six stable and well separated clusters: L-ratio and isolation distance (ID).

A

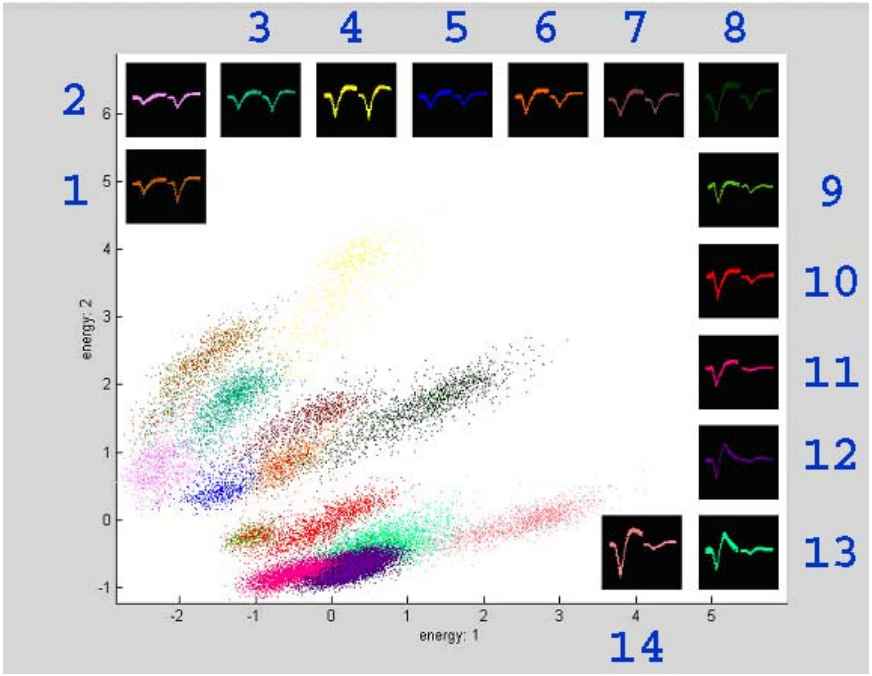


B

| | L-Ratio | Isolation Distance (ID) |
|---|---|---|
| Clust 1 | 0.0764 | 25.9 |
| Clust 2 | 0.0552 | 27 |
| Clust 3 | 0.0518 | 26.9 |
| Clust 4 | 0.0285 | 25 |
| Clust 5 | 0.0563 | 23 |
| Clust 6 | 0.0192 | 31 |
| Clust 7 | 0.044 | 25.9 |
| Clust 8 | 0.0141 | 33.1 |
| Clust 9 | 0.0228 | 27.1 |
| Clust 10 | 0.3007 | 15.7 |
| Clust 11 | 0.0309 | 44.2 |
| Clust 12 | 0.0526 | 24.62 |
| Clust 13 | 1.9556 | 4.8 |
| Clust 14 | 0.0449 | 37 |
| Average | 0.1966 | 26.51571 |

Supporting Figure 8

**Fig. 8.** Fourteen single units were detected and resolved by a single stereotrode. (*A*) Average stereotrode waveforms of the putative separated units and the corresponding energy spike distributions used for this classification. (*B*) Table containing the L-Ratio and isolation distance corresponding to the 14 clusters provides quantitative measures for their quality.

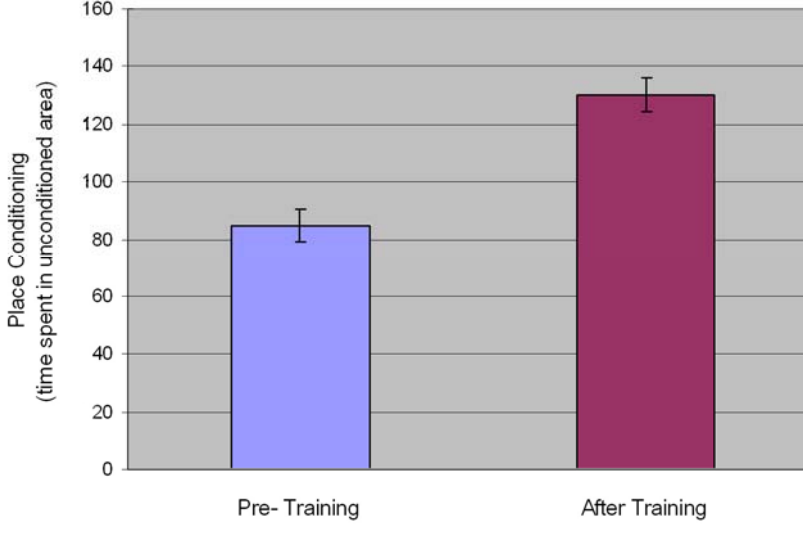
160
140
120
100
80
60
40
20
0
Place Conditioning
(time spent in unconditioned area)
Pre- Training
After Training

Supporting Figure 9

**Fig. 9.** The formation of startling memory in mice as assessed by conditioned place conditioning paradigm. As indicated, the mice spent an equal amount of time (90 s) during the pretraining session (blue bar, 84.9 ± 5.8 s) in both compartments before startle conditioning. However, after startle conditioning, the mice spent significantly more time in the unconditioned (safe) compartment, as shown in the 3-h retention test (red bar, 130.1 ± 5.8 s, $P < 0.0005$; $n = 14$).

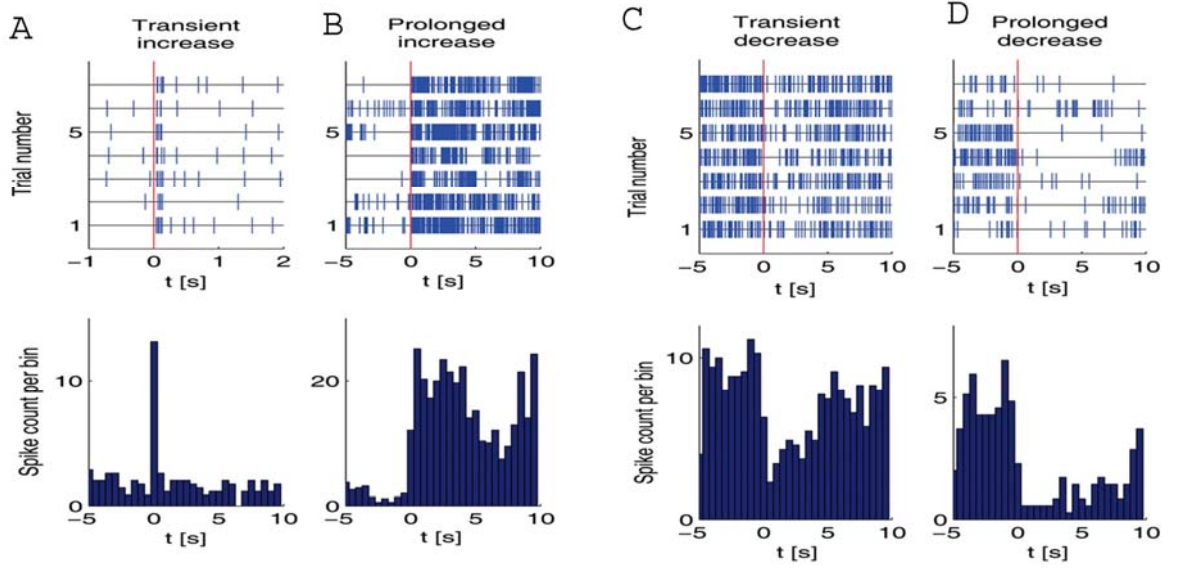
A
Transient increase
B
Prolonged increase
C
Transient decrease
D
Prolonged decrease
Trial number
Spike count per bin
t [s]

Supporting Figure 10

**Fig. 10.** Temporal dynamics of individual units in response to startling events. Spike raster plots (*A--D Upper*, seven repetitions each) and corresponding peri-event histogram (*A--D Lower*, bin width 500 ms) for units exhibiting the four major types of firing changes observed: transient increase (*A*), prolonged increase (*B*), transient decrease (*C*), and prolonged decrease (*D*).

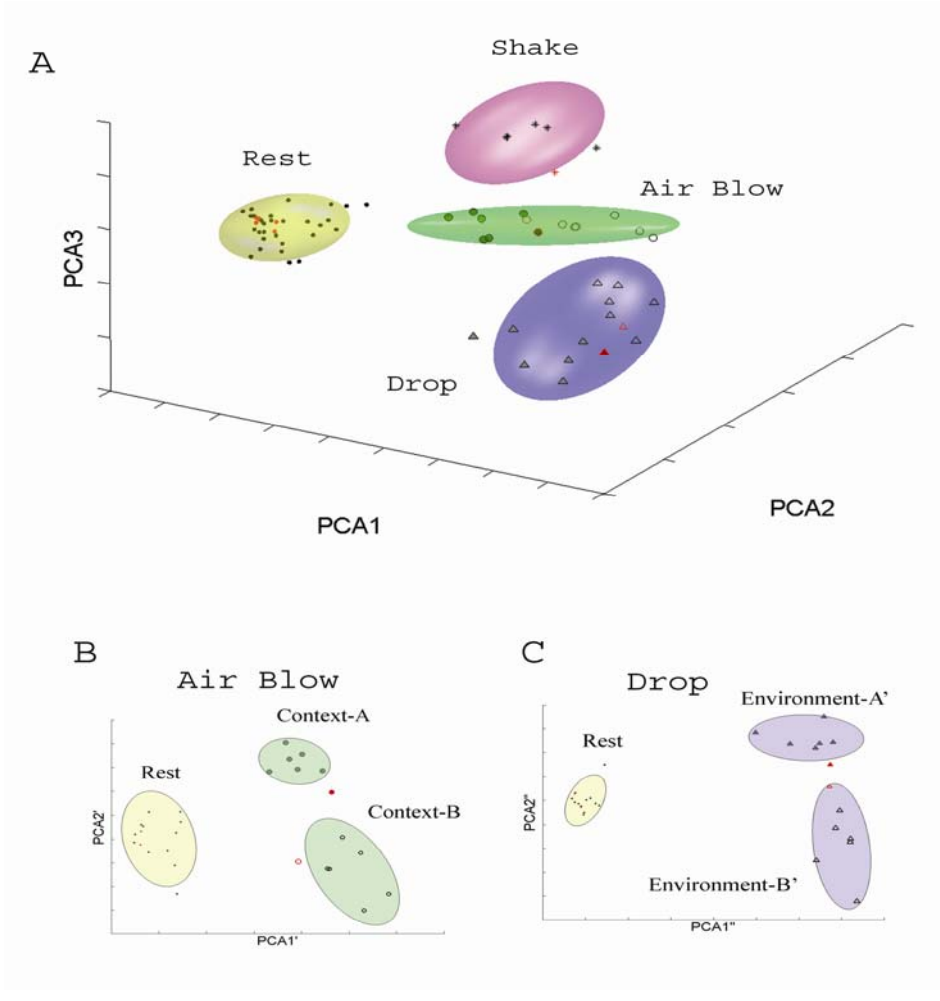
A
Shake
Rest
Air Blow
Drop
PCA3
PCA1
PCA2
B
Air Blow
Context-A
Rest
Context-B
PCA2'
PCA1'
C
Drop
Environment-A'
Rest
Environment-B'
PCA2"
PCA1"

Supporting Figure 11

**Fig. 11.** Classification and visualization of CA1 representations of startle episodes in a low-dimensional encoding subspace generated by principal component analysis (PCA) statistical methods. (*A*) Firing patterns during rest (dots fitted with yellow ellipsoid), air blow (circles fitted with green ellipsoid), drop (triangles fitted with blue ellipsoid) and shake (stars fitted with magenta ellipsoid) epochs are shown after being projected to a three-dimensional space obtained by using the first three eigenvectors obtained from PCA (representative PCA for mouse A is shown here; PCA 1-3 denote the main axes). Both training (dark symbols), and test (red symbols) data points are shown. After the identification of startle types, a subsequent PCA analysis is further used to resolve contexts (full vs. empty symbols) for air-blow context (*B*) and drop context (*C*). For the PCA method, the corresponding startle classes, including their corresponding contexts, have been obtained using hierarchical clustering (with four classes for *A* and three for *B* and *C*).

**Table 2. Prediction power in the principal component analysis-computed encoding subspace for startle type and context**

| Mouse | Rest | Air blow | Air blow in con. A | Air blow in con. B | Drop | Drop in ele. A | Drop in ele. B | Shake |
|---|---|---|---|---|---|---|---|---|
| A | 99 | 99 | 99 | 83 | 99 | 81 | 83 | 98 |
| B | 91 | 84 | 35 | 64 | 89 | 77 | 37 | 84 |
| C | 95 | 92 | 64 | 63 | 98 | 42 | 52 | 91 |
| D | 99 | 87 | 69 | 66 | 94 | 73 | 72 | 80 |

Average performances were computed for mice A, B, C, and D by using 1,000 random combinations of training/test data. Test data was excluded from the training set. To facilitate the comparison with the multiple discriminant analysis (MDA)-based projection method, performances were computed in a similar fashion by using a variation of "leave-one-out" cross-validation method. The startle type was first determined (columns: rest, air blow, drop, and shake), followed by context (con) classification for air blow (context A or B) and drop [elevator (ele) A or B].

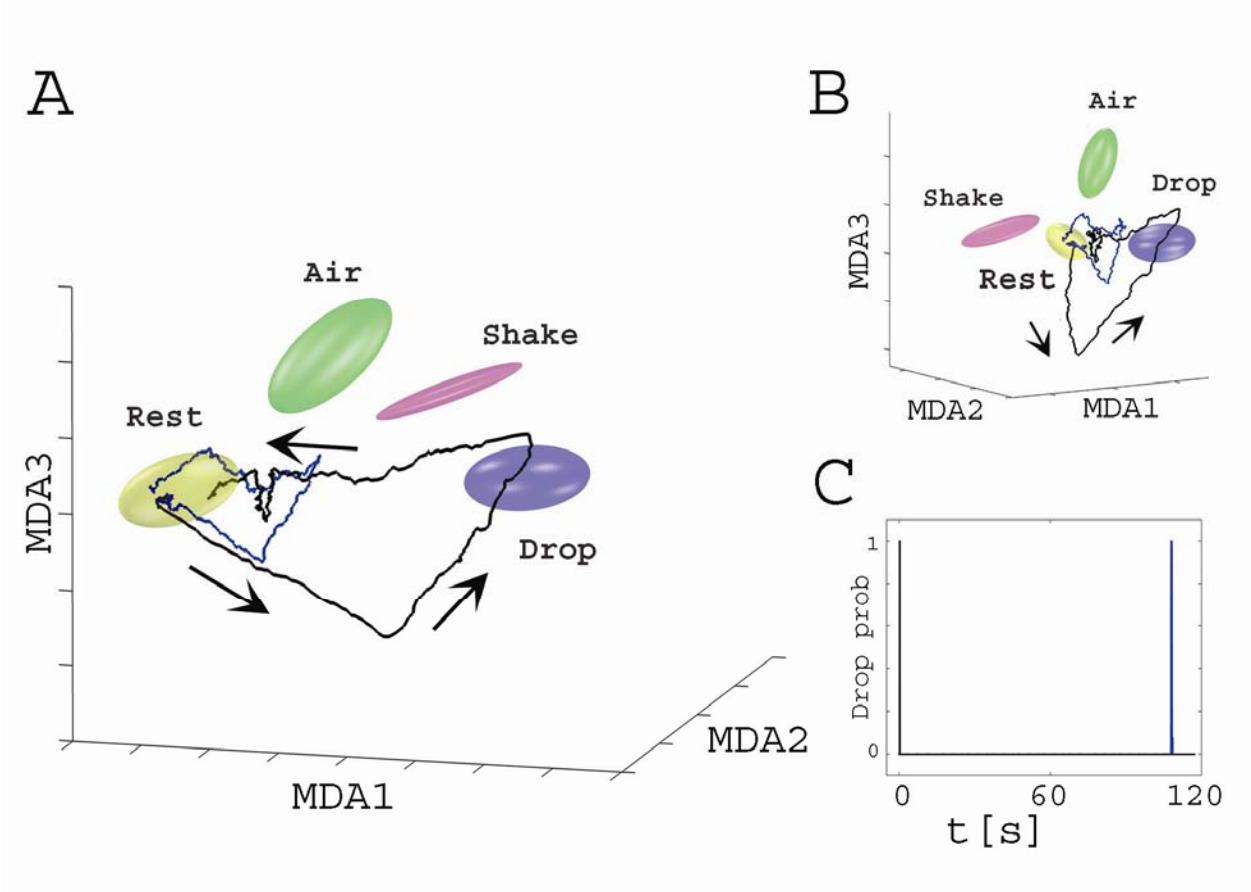
A
Air
Shake
Rest
Drop
MDA3
MDA1
MDA2
B
Air
Shake
Drop
Rest
MDA3
MDA2
MDA1
C
Drop prob
1
0
0
60
120
t [s]

Supporting Figure 12

**Fig. 12.** Dynamical monitoring of ensemble activity and the spontaneous reactivation of startle representations. (*A*) Three-dimensional subspace trajectories of the population activity in the 2 min after a drop startle in mouse A. The initial response to a drop (black line) is followed by one large spontaneous excursions (blue line), characterized by a coplanar, geometrically similar trajectory with a lower amplitude (directionality indicated by arrows). (*B*) The same trajectory from a different orientation. (*C*) The occurrence ($t$ = 107.9 s) of a single reactivation (marked in blue) after the actual startle (in black) ($t$ = 0 s). The vertical axis indicates the drop event classification probability.

**Table 3. Encoding power of neural cliques**

| Selected pool of neurons | Rest | Air blow | Air blow in cont A | Air blow in cont B | Drop | Drop in elev A | Drop in elev B | Shake |
|---|---|---|---|---|---|---|---|---|
| 40 unresponsive neurons | 56 | 39 | 11 | 6 | 37 | 18 | 15 | 31 |
| 40 unresponsive + 10 general startle neurons | 98 | 53 | 21 | 34 | 79 | 48 | 52 | 53 |
| 40 unresponsive + 10 general startle + 10 drop neurons | 99 | 84 | 38 | 66 | 99 | 83 | 82 | 70 |
| 40 unresponsive + 10 general startle + 10 drop +10 air + 10 shake neurons | 99 | 99 | 86 | 95 | 99 | 93 | 91 | 92 |
| 10 general startle + 10 drop + 10 air + 10 shake neurons | 99 | 99 | 88 | 98 | 99 | 96 | 92 | 93 |

Using the same parameters and procedures as in Table 1, the startle type was first determined (rest, air blow, drop, and shake), followed by context (cont) classification for air blow (context A or B) and drop [elevator (elev) A or B] for mouse A. Although the 40 unresponsive neurons yielded poor generalization performances (row 1), sequential addition of 10 general startle clique neurons (row 2), 10 drop clique neurons (row 3), and 10 air clique and 10 shake clique neurons (row 4), to the initial 40 unresponsive neurons pool gradually increased the classification results. In addition, the use of the 40 clique neurons (row 5) generates reliable classification performances.

**Table 4. Prediction power in the clique subspace for startle type and context**

| Mouse | Rest | Air blow | Air blow in cont A | Air blow in cont B | Drop | Drop in elev A | Drop in elev B | Shake |
|---|---|---|---|---|---|---|---|---|
| A | 99 | 99 | 99 | 94 | 99 | 91 | 98 | 98 |
| B | 99 | 99 | 94 | 95 | 97 | 92 | 93 | 93 |
| C | 99 | 99 | 91 | 92 | 99 | 80 | 87 | 90 |
| D | 99 | 90 | 91 | 75 | 96 | 66 | 75 | 83 |

Binary codes hit ratio for episodic events detection were evaluated by using 1,000 random combinations of training/test data for each mouse. The startle type was first determined (rest, air blow, drop, and shake), followed by context (cont) classification for air-blow (context A or B) and drop [elevator (elev) A or B]. The analysis is based on the activation of the binary codes (threshold crossing) obtained by remapping the multiple discriminant analysis (MDA)-encoding subspace into the clique subspace by using data sets from simultaneously recorded 260, 210, 148, and 138 individual CA1 units in mice A, B, C, and D, respectively.

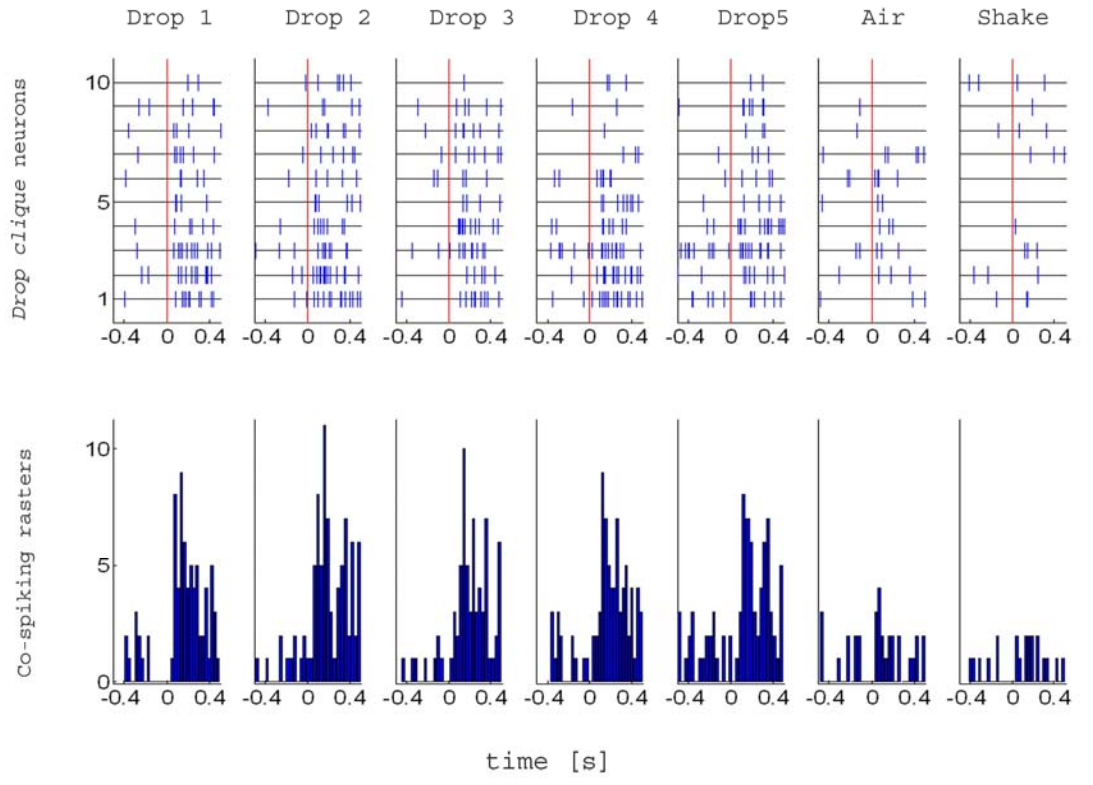
Drop 1
Drop 2
Drop 3
Drop 4
Drop5
Air
Shake
Drop clique neurons
10
5
1
-0.4 0 0.4
Co-spiking rasters
10
5
0
time [s]

Supporting Figure 13

**Fig. 13.** Real-time encoding robustness exhibited by neural cliques. Drop neural clique is showed here as an example. Spike rasters and collective peri-event histogram responses of the top 10 drop clique neurons during startle events (five drop, one air, and one shake). As evident from the histogram plots, neural summed responses are considerably less variable from trial to trial than their individual components. These responses are specific to drop events because air blow and shake episodes elicit no significant responses (last two insets on right). Reliable cospiking of neurons in the cliques is preserved at the finer time scale (20-30 ms).

A

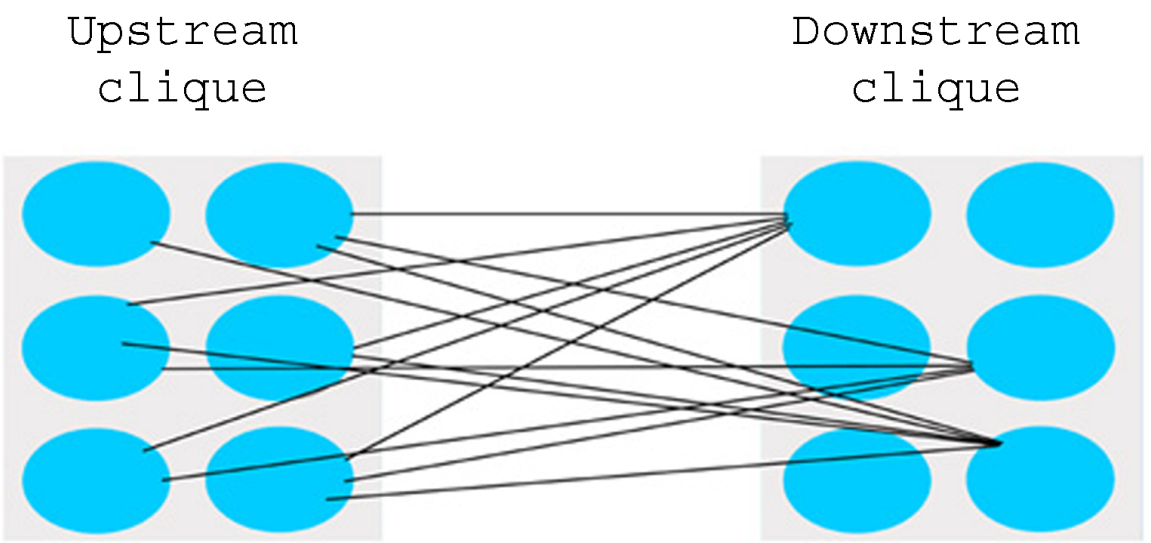


$$f(t) = h(\sum_{n=1}^{N} w_n R_n(t))$$

B

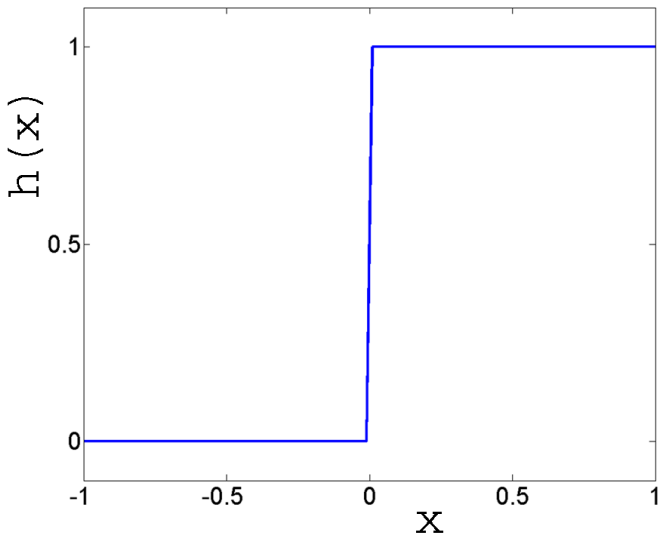


C

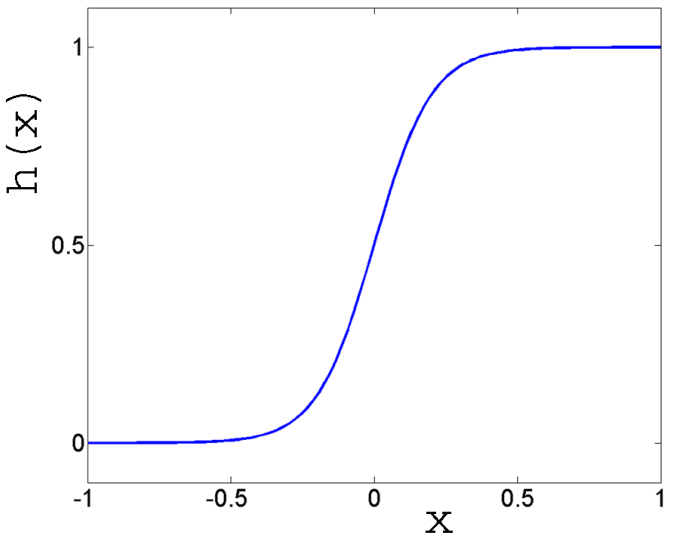

Supporting Figure 14

**Fig. 14.** Mathematical description of the neural clique activation function. (*A*) Illustration of how cospiking of member neurons in the upstream clique can drive the activation of the downstream clique. Activation of the downstream neural clique can be conveniently assessed by step or sigmoid threshold functions. This type of transfer of information can be repeatedly implemented across multiple network layers. (*B*) Graphs of a step threshold function. (*C*) Graph of a sigmoid activation function $h(x) = 1/(1 + \exp(-\beta x))$, $\beta = 10$.